ELSEVIER

Biophysical Chemistry 65 (1997) 75–83

Biophysical Chemistry

Structure and thermodynamics of nonideal solutions of colloidal particles: Investigation of salt-free solutions of human serum albumin by using small-angle neutron scattering and Monte Carlo simulation

Bo Sjöberg [a,*], Kell Mortensen [b]

[a] *Department of Medical Biochemistry, University of Göteborg, Medicinaregatan 9, S-413 90 Göteborg, Sweden*
[b] *Physics Department, Risø National Laboratory, Box 49, DK-4000, Roskilde, Denmark*

Received 18 August 1996; revised 28 October 1996; accepted 30 October 1996

Abstract

The understanding of the structural and thermodynamic properties of moderately or highly concentrated solutions is fundamental, e.g., in medicine and biology and also in many technical processes. In this work, we have used the small-angle neutron scattering method (SANS), in combination with Monte Carlo simulation, to study salt-free solutions of human serum albumin (HSA) in the concentration range up to 0.26 g ml^{-1}. The model calculations of the theoretical SANS intensities are quite general, thus avoiding the approximation that the relative positions and orientations of the particles are independent of each other. The computation of the theoretical intensities also includes the calculation of a 'thermodynamic' intensity scattered at zero angle, which is obtained via the nonideal part of the chemical potential. The latter quantity is obtained by applying the test particle method during the Monte Carlo simulations. It is found that the SANS data can be explained by a model where the HSA molecules behave as hard ellipsoids of revolution with semiaxes $a = 6.8$ nm, $b = c = 1.9$ nm. In addition to the hard core interaction, the particles are also surrounded by a soft, repulsive rectangular-shaped potential which is spherically oriented around the particles. The combination of SANS and statistical thermodynamics also allows a determination of the nonideal part of the chemical potential and the activity coefficient of HSA. As expected the activity coefficient deviates strongly from the value one (several powers of ten) already at fairly low concentrations; the effects are comparable to, or even larger than, for instance hydrophobic or van der Waals interaction. © 1997 Elsevier Science B.V.

Keywords: Nonideal solutions; Small-angle neutron scattering; Monte Carlo simulation; Human serum albumin

1. Introduction

Although macromolecular and other colloidal particles are commonly studied in dilute solutions, or in the crystalline state, they often occur at moderate or high concentrations in natural environments. For instance, the macromolecular concentration within a

Abbreviations: SANS, small-angle neutron scattering; HSA, human serum albumin

* Corresponding author. Tel.: +46-317733458; e-mail: bo.sjoberg@medkem.gu.se.

PII S0301-4622(96)02251-X

typical in vivo cell is about 0.25 g ml^{-1}; the corresponding value for blood plasma is slightly lower, about 0.08 g ml^{-1}. Also, technical processes in food industry, ore flotation, paint industry, cosmetics, etc., are often based on moderately or highly concentrated solutions. In many such processes, the forces between the particles are altered in order to produce new properties of the systems, to alter the way they stick to surfaces, etc.

In spite of the fact that knowledge of both thermodynamic and structural properties of moderately or highly concentrated systems is very important, this is still to a great extent a neglected area of chemistry. It is thus desirable to develop both experimental and theoretical methods for their exploration, to see how the properties of the system depends upon parameters like pH, ionic strength, surface charge, temperature, etc.

In a previous investigation [1], we have used the SANS method in combination with Monte Carlo simulations to investigate solutions of HSA in D_2O solutions containing 1.08 M NaCl. In the present work, we have expanded the measurements to include salt-free solutions. Compared with the previous investigation we have also modified the calculations of the theoretical SANS intensity in order to avoid the approximation that the relative positions and orientations of the particles are independent of each other. The computation of the theoretical intensity also includes the calculation of a 'thermodynamic' intensity scattered at zero angle, which is obtained via the nonideal part of the chemical potential.

It is found that the SANS data obtained from the salt-free solutions can be explained by a rather simple model where the HSA molecules behave as hard ellipsoids of revolution with semiaxes $a = 6.8$ nm, $b = c = 1.9$ nm. In addition to the hard core interaction, the particles are also surrounded by a soft, repulsive rectangular-shaped potential which is spherically oriented around the particles. The combination of SANS and statistical thermodynamics also allows a determination of the nonideal part of the chemical potential and the activity coefficient of HSA. As expected the activity coefficient deviates strongly from the value one (several powers of ten) already at fairly low concentrations; the effects are comparable to, or even larger than, for instance hydrophobic or van der Waals interaction.

The advantage of the combination of Monte Carlo simulation and the SANS method is that complete general models, both regarding particle shape and interaction potential, can be considered. We can introduce more realistic molecular shapes and we can avoid the assumption of spherical, or even point shaped particles, which have been made in most previous investigations. Furthermore, the method of analysis presented also offers a possibility to determine thermodynamic parameters, like for instance chemical potentials and activity coefficients.

2. Materials and SANS measurements

The HSA samples used in this investigation were of the same origin (Sigma, product A-8763) and they were prepared and analyzed as described in the previous publication [1]. The only difference is that, in this investigation, HSA was dissolved directly in 99.9% D_2O, without any addition of salt or buffer media. According to the manufacturer's specification, the HSA powder is essentially salt-free. The apparent pD value of the HSA solutions, measured with a pH electrode filled with saturated KCl in H_2O, was 7.1. The electrode was calibrated against standard buffers in H_2O.

The H_2O content of the HSA powder (6%), as well as the labile hydrogens of the HSA, results in a varying D_2O content of the solvents from 93.8%, for the highest HSA concentration, to 99.8% for the lowest concentration used. In order to equilibrate the hydrogen–deuterium exchange, at least 24 h elapsed before the SANS measurements were performed. In the calculations described below we assume that the shape of the HSA molecules can be approximated as an ellipsoid of revolution with semiaxes $a = 6.8$ nm, $b = c = 1.9$ nm and that the molecular weight is 67120 [2]. The model for the HSA molecule was obtained as a result of a traditional shape analysis where different types of three-axial bodies were fitted directly to SANS data extrapolated to zero concentration [1].

The SANS data were collected by using the facility at Risø National Laboratory, Denmark, set at sample-to-detector distances equal to 2.50 and 6.00 m and a neutron wavelength $\lambda = 0.35$ nm ($\Delta\lambda/\lambda =$ 16%, full width at half maximum). The data were

corrected for background and detector nonuniformities, and transformed to the radial form, as described previously [1]. In the background correction, we subtracted the intensity recorded from D_2O having a H_2O content corresponding to the sample under consideration. The temperature of the 0.2 cm quartz cuvettes used as sample containers was kept at 21.0°C.

3. The Monte Carlo simulations

In this work, we have used canonical ensemble Monte Carlo simulations [3] in order to calculate both the theoretical intensity and the nonideal part of the chemical potential for the models. The latter quantity is used in order to obtain 'thermodynamic' values of the intensity scattered at zero angle.

The model system for the simulations consists of a basic cubic cell of side length L and volume V containing N ellipsoids of revolution with semiaxes [1] $a = 6.8$ nm, $b = c = 1.9$ nm. Several types of pairwise interaction energies $U(r)$ have been tested. The model found which gives the best fit to the experimental SANS data consists of two parts: (1) The ellipsoids are impenetrable, that is $U(r) = \infty$ when the ellipsoids overlap. (2) They are surrounded by a spherical soft repulsive potential $U(r) = E_2$ for center–center distances $r \leq E_1$, $U(r) = 0$ for $r > E_1$; E_1 and E_2 being two constants which will be determined as described below.

The solvent is treated as a featureless continuum. The volume fraction of the cell occupied by the particles is $\eta = Nv/V$, where the particle volume $v = 4\pi ab^2/3$. Surface effects due to the limited size of the cell were eliminated, as far as possible, by using the periodic boundary condition [4,5].

Starting configurations for the highest particle densities used were generated by filling the cell with ellipsoids of revolution in nonoverlapping random positions and with random orientations. Marsaglia's method [6] was used in order to generate random orientations of the unique axis of the ellipsoids. The Vieillard-Baron criterion [7] was used to check for overlapping of the ellipsoids. For the lower particle densities we started with a high density sample and just used a subset of randomly selected particles.

A standard Metropolis Monte Carlo algorithm [3] has been used in order to generate random configurations of the system. The simulation process always started with at least 10^5 Monte Carlo steps, in order to equilibrate the system. After between 10^4 to 10^5 Monte Carlo steps, a configuration was chosen and $I(Q)$ was calculated as described in Section 4, $Q = (4\pi \sin \xi)/\lambda$, where ξ is half the scattering angle and λ the neutron wavelength. In addition to $I(Q)$ we also calculated the nonideal part of the chemical potential $\beta\mu^{ni}$, at this stage of the Monte Carlo simulation, by using the method described in Section 5. This important function is of course very interesting in itself; it is used here also to calculate the intensity scattered at zero angle, $I(0)$. As usual $\beta = 1/(kT)$, k being Boltzmann's constant and T the absolute temperature.

The final values of $I(Q)$ consisted of averages taken over from 10^3 to 10^5 individual configurations, depending on the number of particles in the basic cell. Compared with $I(Q)$ the calculation of the chemical potential can be performed much more easily and, consequently each average of $\beta\mu^{ni}$ consisted of at least 5×10^5 individual values. In order to check the stability of the simulations we have varied all the parameters within wide limits. The side length L of the cell was chosen between 50 to 200 nm and the number of particles varied between 88 and 704. The calculation of both $I(Q)$ and $\beta\mu^{ni}$ was found to be surprisingly stable. In multiple calculations, we always arrived at the same result, within the statistical errors.

For the final models, we have also calculated averages of the pair distribution function $P(r)$ by choosing configurations about 5×10^5 Monte Carlo steps apart and calculating the number of center–center distances falling between $r - 1/2\Delta r$ and $r + 1/2\Delta r$. In order to correct for the finite size of the basic cell, the result was divided with the distance distribution function for a cube [8].

4. Calculation of the scattered intensity

In the previous investigation [1], the calculation of the theoretical intensity was based on the assumption that the relative orientations and positions of the particles are independent of each other. Here, we have used another approach where this assumption can be avoided.

For each configuration generated as described above we first calculated the intensity scattered from the cell with the particles in fixed positions and orientations by using the equation

$$I(\boldsymbol{Q}) = \left\{ \sum_{k=1}^{N} F_k(\boldsymbol{Q}) \cos(\boldsymbol{Q}\boldsymbol{R}_k) \right\}^2 + \left\{ \sum_{k=1}^{N} F_k(\boldsymbol{Q}) \sin(\boldsymbol{Q}\boldsymbol{R}_k) \right\}^2 \quad (1)$$

where $F_k(\mathbf{Q})$ is the structure factor of the kth ellipsoid, $\mathbf{Q}$ the scattering vector and $\mathbf{R}_k$ the position vector of the ellipsoid. The advantage of using Eq. (1) instead of the double summation of $F_k F_j \cos[\mathbf{Q}(\mathbf{R}_k - \mathbf{R}_j)]$ normally used, is that the computation of Eq. (1) can be made considerably faster, especially when the number of particles N is large.

Next, assuming that the sample is composed of very many cells which can take all possible orientations we calculate the average

$$I(Q) = \frac{1}{4\pi} \int_{\theta=0}^{\pi} \int_{\varphi=0}^{2\pi} I(\boldsymbol{Q}) \mathrm{d}\varphi \sin\theta \mathrm{d}\theta \quad (2)$$

where θ is the colatitude and φ the longitude of $\mathbf{Q}$ in a spherical polar coordinate system.

The above calculations (Eq. (1) and Eq. (2)) were repeated for each individual configuration chosen during the Monte Carlo procedure. The final intensity, $I_{\mathrm{tot}}(Q)$, consisted of an average taken over from 10^3 to 10^5 individual configurations. The intensity $I_{\mathrm{tot}}(Q)$ is normalized so that $I_{\mathrm{tot}}(0) = N^2$.

At very small Q-values ($Q \leq 2\pi/L$) the volume scattering from the Monte Carlo cell dominates $I_{\mathrm{tot}}(Q)$, whereas at larger Q-values ($Q > 2\pi/L$) the shape of the particles and their arrangement dominates $I_{\mathrm{tot}}(Q)$; L being the side length of the cell. The volume scattering was eliminated by taking the difference

$$I(Q) = \frac{I_{\mathrm{tot}}(Q) - N^2 I_{\mathrm{cell}}(Q)}{N} \quad (3)$$

where $I_{\mathrm{cell}}(Q)$ is the scattering from a cube [9], having the dimensions of the cell used in the Monte Carlo simulations. In Eq. (3) we also define a normalization by dividing with N so that $I(0) = 1$ for an ideal solution, independently of N.

Finally, $I(Q)$ was smeared with the wavelength distribution used during the SANS measurements and compared with the experimental data.

5. Zero angle scattering

The drawback with the above calculation of $I(Q)$ is that, at small Q-values ($\leq 2\pi/L$), $I_{\mathrm{tot}}(Q)$ and $N^2 I_{\mathrm{cell}}(Q)$ are of equal size and the relative errors in $I(Q)$ will be quite large when taking the difference in Eq. (3). When $Q = 0$ these quantities are equal and $I(0) \equiv 0$. Consequently, $I(0)$, for the theoretical model under consideration, can be obtained only by extrapolation to zero angle, which leads to a relatively large uncertainty. One way to reduce this uncertainty is to increase the dimensions of the cell. This will, however, drastically increase the computation time.

There is, however, an alternative route by which $I(0)$ can be calculated. That is directly from the thermodynamic properties of the model under consideration. This can be made quite easily and $I(0)$ will be obtained as a by-product during the Monte Carlo simulation. As follows below this statistical thermodynamic approach, in combination with SANS, also allows the determination of the nonideal part of the chemical potential for the samples investigated. Furthermore, the knowledge of $I(0)$ also provides a support when constructing the theoretical $I(Q)$ at small values of Q.

By combining the relations between $I(0)$, the isothermal compressibility and the chemical potential, it can be shown that [10]

$$I(0) = \left[N \left(\frac{\partial(\beta\mu)}{\partial N} \right)_{V,T} \right]^{-1} \quad (4)$$

The chemical potential μ can be written as the sum of two terms

$$\mu = \mu^{\mathrm{id}} + \mu^{\mathrm{ni}} \quad (5)$$

TThe first term is the ideal part, where

$$\beta\mu^{\mathrm{id}} = \ln\left\{ \frac{N\Lambda^3}{V} \right\} \quad (6)$$

where the de Broglie thermal wavelength $\Lambda = (\beta h^2/2\pi m)^{1/2}$, h = Planck's constant and m = the

mass of the particles. The second term of Eq. (5), the nonideal part, contains all the contributions which arise from the interactions between the particles. Widom has shown that [11,12]

$$\beta\mu^{ni} = -\ln\langle\exp(-\beta\Psi(\mathbf{r}))\rangle \quad (7)$$

$\Psi(\mathbf{r})$ is the work needed to bring a test particle from infinity to a point $\mathbf{r}$ in the fluid. The average $<\exp(-\beta\Psi(\mathbf{r}))>$ is obtained during the Monte Carlo simulations (Section 3) by averaging over all points $\mathbf{r}$ and all possible canonical configurations of the N particles in the system.

By combining Eq. (4), Eq. (5) and Eq. (6) it can be shown that

$$I(0) = \left[1 + \eta\left(\frac{\partial(\beta\mu^{ni})}{\partial\eta}\right)_{V,T}\right]^{-1} \quad (8)$$

Here, $\eta = Nv/V$ = the volume fraction of the sample occupied by the particles, v = the volume of a single particle. Eq. (8) is normalized so that $I(0) = 1$ for an ideal system.

For the different models described below, $\beta\mu^{ni}$ values were calculated from Eq. (7) as a function of η and fitted to polynomial functions of the type

$$\beta\mu^{ni} = A_1\eta + A_2\eta^2 + A_3\eta^3 + A_4\eta^4 \quad (9)$$

as described in Ref. [13].

By combining Eq. (8) and Eq. (9), it follows that

$$I(0) = \left[1 + A_1\eta + 2A_2\eta^2 + 3A_3\eta^3 + 4A_4\eta^4\right]^{-1} \quad (10)$$

The $I(0)$-values obtained by the above procedure have been used as a support when calculating the theoretical $I(Q)$-functions of Fig. 1 below. Even if the calculation of $I(Q)$ from Eq. (3) is quite inaccurate for $Q \leq 2\pi/L$, the construction of $I(Q)$ can be made rather accurately by interpolating between the thermodynamic $I(0)$ and the $I(Q)$-values obtained from Eq. (3) in the more accurate region.

6. Results and discussion

The experimental SANS data obtained from the salt-free HSA samples are shown in Fig. 1. It follows that there is a pronounced deviation from thermodynamic ideality already at the lowest concentration, 0.0049 g ml^{-1} (Sample A). This deviation increases with the HSA concentration. For thermodynamically ideal solutions we would obtain Gaussian shaped $I(Q)$ curves (at small Q) with their maxima at $Q = 0$. All the intensities in Fig. 1 have their maxima at $Q > 0$. As expected the Q value where the maximum occur, Q_{max}, increases when the concentration becomes larger. That is, there is an inverse relationship between Q_{max} and the average interparticle distances in solution.

In Fig. 1, we also make a comparison with the intensities obtained by Monte Carlo simulation for the best fitting model found. The model consists of the following: (1) The HSA molecules are approximated as ellipsoids of revolution with semiaxes a = 6.8 nm and $b = c$ = 1.9 nm. (2) The ellipsoids behave as hard bodies, that is $U(r) = \infty$ if they overlap. (3) In addition to the hard body interaction there is also a soft spherical repulsive potential $U(r) = E_2$ for center–center distances $r \leq E_1$, $U(r) = 0$ for $r > E_1$.

Values of E_1 and E_2 are given in Table 1. It follows that the energy E_2 is relatively constant about 3.5 kT. The values of E_1, on the other hand, varies inversely with concentration from about 7.2 to 14.5 nm.

We were surprised to see that the above, rather primitive, model can give such a good explanation of the experimental data. The fits at the lower concentrations are excellent although, for the more concentrated solutions, the deviations are larger than the statistical errors of the measurements, which are approximately equal to the size of the symbols in Fig. 1. The reason for this deviation might be that the test particle method fails, and gives slightly too large values of $\beta\mu^{ni}$, and consequently too small values of $I(0)$, when the solution becomes more crowded. Our main criterion in the fitting procedure was to obtain coinciding maxima in the experimental and theoretical intensities.

It should also be mentioned that we have tested several other types of $U(r)$ functions but best fits were obtained for the model described above. For instance, we did not succeed to fit the exponential type of function which was used in the previous investigation [1] of HSA solutions containing 1.08 M NaCl.

One must, of course, ask whether the conforma-

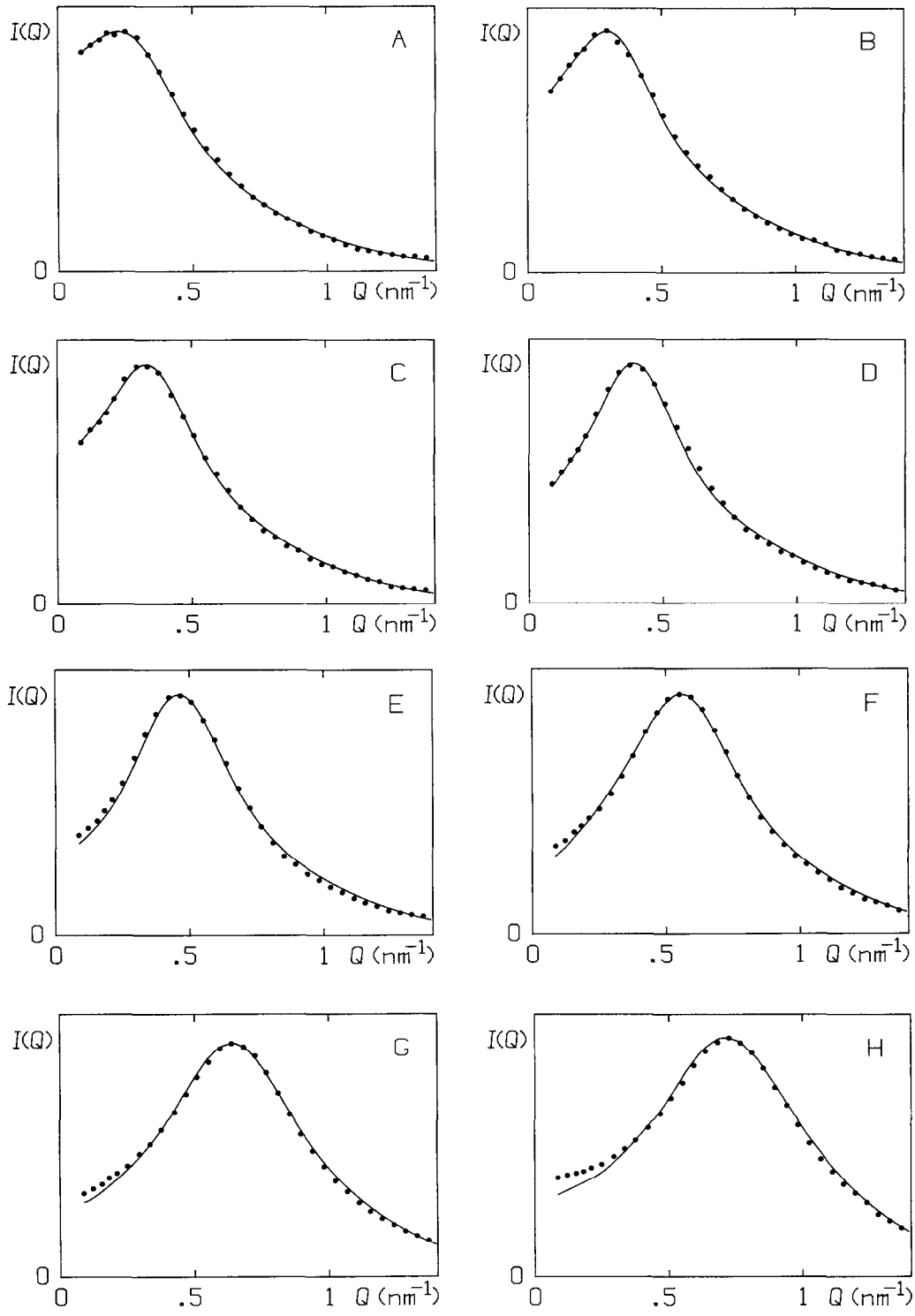
I(Q)
A
0
0
.5
1 Q (nm⁻¹)
I(Q)
B
0
0
.5
1 Q (nm⁻¹)
I(Q)
C
0
0
.5
1 Q (nm⁻¹)
I(Q)
D
0
0
.5
1 Q (nm⁻¹)
I(Q)
E
0
0
.5
1 Q (nm⁻¹)
I(Q)
F
0
0
.5
1 Q (nm⁻¹)
I(Q)
G
0
0
.5
1 Q (nm⁻¹)
I(Q)
H
0
0
.5
1 Q (nm⁻¹)

Table 1
Parameters of the salt-free HSA samples used

Sample	C (g ml^{-1})	η	E_1 (nm)	E_2 (kT-units)	$I(0)$	$\beta\mu^{ni}$
A	0.00490	0.00452	14.5	3.0	0.594	0.61
B	0.00956	0.00882	13.8	3.0	0.421	1.15
C	0.0149	0.0137	13.0	3.0	0.340	1.57
D	0.0300	0.0277	12.0	3.0	0.212	2.83
E	0.0577	0.0532	10.5	3.5	0.113	4.34
F	0.116	0.107	9.1	4.0	0.081	7.5
G	0.190	0.175	8.0	4.0	0.062	10
H	0.259	0.239	7.2	4.0	0.040	12

C is the concentration, η is the volume fraction occupied by HSA, E_1 and E_2 are constants defining the interaction between the particles, $I(0)$ is the intensity scattered at zero angle (normalized to be equal to one for an ideal solution) and $\beta\mu^{ni}$ is the nonideal part of the chemical potential.

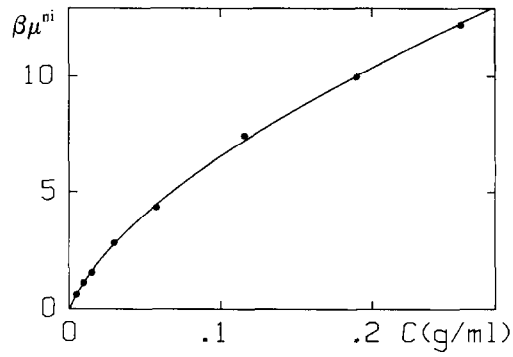

Fig. 2. Values of $\beta\mu^{ni}$ plotted as a function of HSA concentration C for samples A–H. As usual $\beta = 1/(kT)$, k being Boltzmann's constant and T the absolute temperature; μ^{ni} is the nonideal part of the chemical potential. The curve represents an arbitrary function ($Y = 72.75X^{0.5169} - 43.76X^{0.4479}$) which was found useful in order to interpolate the data.

tion of HSA is concentration dependent. This question cannot be completely resolved from SANS data alone. We can only say that there is no indication of a large conformational change. This conclusion is based on two arguments: (a) the whole data set can be explained by a simple few parameter model and (b) when plotting $I(Q)/C$, for large values of Q where the interparticle effect is negligible but the curves are very sensitive regarding conformation, we obtain coinciding curves.

The approach used in this work also enables a determination of the nonideal part of the chemical potential of HSA for the samples used. Values of $\beta\mu^{ni}$ are given in Table 1. They are also plotted as a function of concentration in Fig. 2. From the relationship

$$f = \exp(\beta\mu^{ni}) \quad (11)$$

we can also calculate the activity coefficient f and we obtain values ranging from 1.8 up to about 10^5. The upper limit of f must be treated with caution because of the deviations between the experimental and theoretical intensities for the highest concentrations in Fig. 1. We have, however, a clear indication that he activity coefficient can deviate very strongly (several powers of ten) from the value one, already at rather low concentrations.

These data are in qualitative agreement with results obtained by for instance measurements of the osmotic pressure. It has been known for a long time that protein solutions, especially at low salt concentrations, show abnormal osmotic behaviour [14,15]. The results also give an idea about the errors which occur when it is assumed that $f = 1$, which is usually the case in equilibrium and kinetic studies in biochemistry. Great care should always be taken when one extrapolates results obtained in dilute solutions to the conditions in blood plasma or in cytoplasm. For instance, in a 0.2 g ml^{-1} HSA solution we obtain an energy corresponding to about 26 kJ mol^{-1}. That is a value which is comparable to, or even larger than the energies of hydrophobic or van der Waals interaction. In spite of that, most textbooks in biochemistry ignore the effects of macromolecular crowding.

It should also be mentioned that, in a mixture of several components, it is the total macromolecular concentration which is critical and it will have great influence also upon a single component which is

Fig. 1. Experimental SANS intensities obtained for the salt-free HSA samples. The concentrations of samples A–H are given in Table 1. The curves are the intensities obtained by Monte Carlo simulation for the models described in the text. The scattered neutron intensities $I(Q)$ are plotted on relative scales; $Q = (4\pi \sin\xi)/\lambda$, where ξ is half the scattering angle and λ the neutron wavelength.

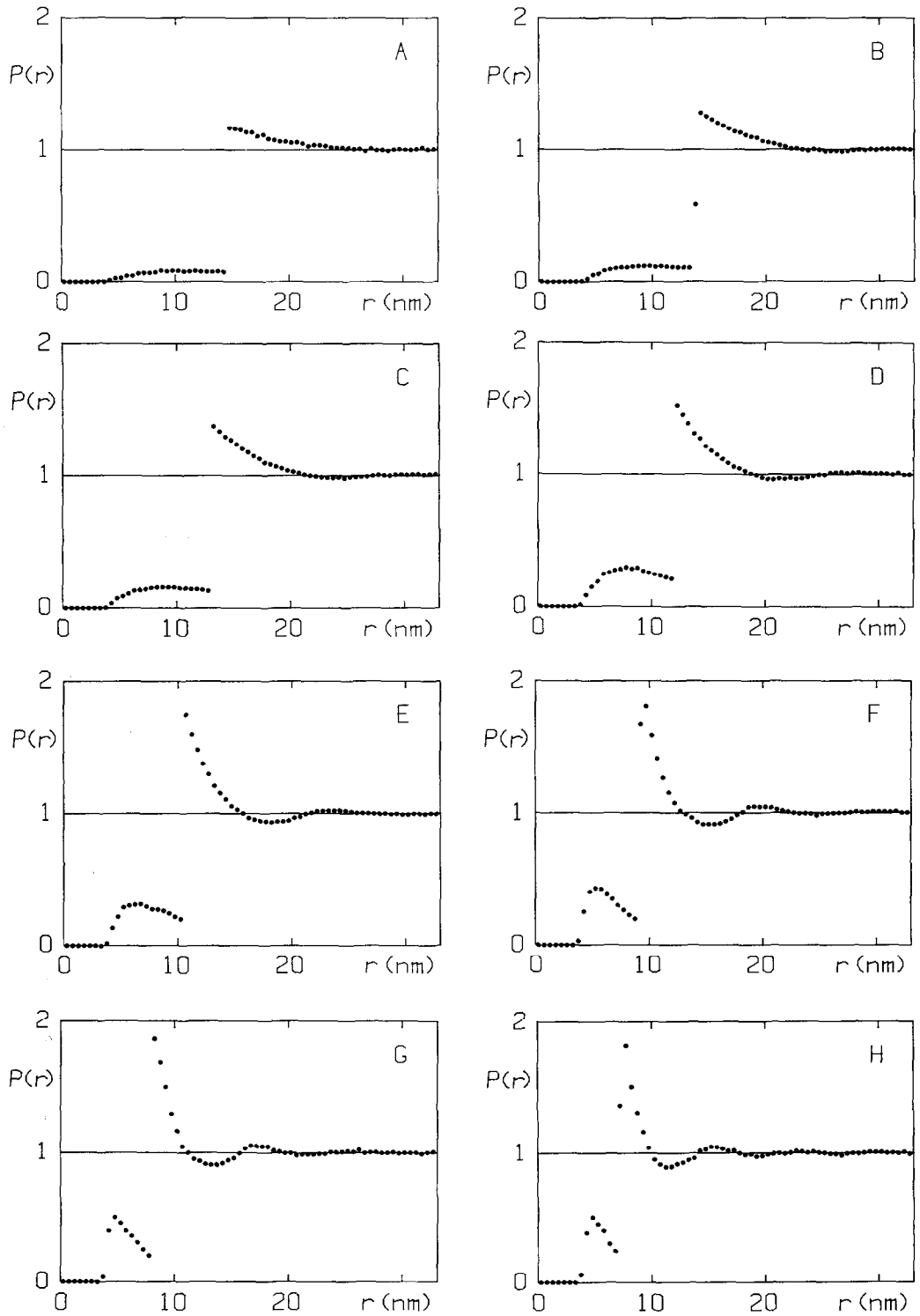

Fig. 3. The pair distribution function $P(r)$ calculated by Monte Carlo simulations for the best fitting models corresponding to samples A–H; r is the distance between the particles.

present at low concentration [16]. Furthermore, the results also demonstrate that great care should always be taken to eliminate interparticle scattering effects in traditional small-angle X-ray and neutron scattering investigations where one is interested only in the shape of the particles.

In Fig. 3, we show the pair distribution function $P(r)$. It follows that there is a sharp maximum in $P(r)$ when $r \approx E_1$. As expected this maximum occurs at smaller r values when the samples become more crowded. For the higher concentrations, there is also a small maximum in $P(r)$ when r is slightly larger than the double b-axis of the ellipsoids which indicates that the particles also have a tendency to order themselves very close to each other. Finally, we can see that there is a substantial ordering in the samples already at rather low concentrations.

Acknowledgements

This work was supported by a grant from the Magn. Bergvall Fund.

References

[1] B. Sjöberg and K. Mortensen, Biophys. Chem. 52 (1994) 131.
[2] T. Peters, Jr., Adv. Protein Chem. 37 (1985) 161.
[3] M.P. Allen and D.J. Tildesley, Computer Simulation of Liquids (Clarendon Press, Oxford, 1987).
[4] N. Metropolis, A.W. Rosenbluth, M.N. Rosenbluth, A.H. Teller and E.J Teller, J. Chem. Phys. 21 (1953) 1087.
[5] W.W. Wood and F.R. Parker, J. Chem. Phys. 27 (1957) 720.
[6] G. Marsaglia, Ann. Math. Stat. 43 (1972) 645.
[7] J. Vieillard-Baron, J. Chem. Phys. 56 (1972) 4729.
[8] J. Goodisman, J. Appl. Cryst. 13 (1980) 132.
[9] P. Mittelbach and G. Porod, Acta Phys. Aus. 14 (1961) 185.
[10] J.-P. Hansen and I.R. McDonald, Theory of Simple Liquids (Academic Press, London, 1986).
[11] B. Widom, J. Chem. Phys. 39 (1963) 2808.
[12] B. Widom, J. Phys. Chem. 86 (1982) 869.
[13] B. Sjöberg, in preparation.
[14] S.P.L. Sørensen, Compt. Rend. Trav. Lab. Carlsberg 12 (1917) 255.
[15] G.S. Adair, Proc. R. Soc. London, Ser. A 120 (1928) 573.
[16] S.B. Zimmerman and A.P. Minton, Annu. Rev. Biophys. Biomol. Struct. 22 (1993) 27.